NANO LETTERS

2009
Vol. 9, No. 11
3860-3866

Ferromagnetic GaAs/GaMnAs Core−Shell Nanowires Grown by Molecular Beam Epitaxy

Andreas Rudolph,[†] Marcello Soda,[†] Matthias Kiessling,[†] Tomasz Wojtowicz,[‡] Dieter Schuh,[†] Werner Wegscheider,[†,§] Josef Zweck,[†] Christian Back,[†] and Elisabeth Reiger*,[†]

Institute for Experimental and Applied Physics, University of Regensburg, Universitätsstrasse 31, D-93053 Regensburg, Germany, Institute of Physics, PAS, Al. Lotników 32/46, 02-668 Warsaw, Poland, and Solid State Physics Laboratory, ETH Zurich, 8093 Zurich, Switzerland

Received June 27, 2009; Revised Manuscript Received August 12, 2009

ABSTRACT

GaAs/GaMnAs core−shell nanowires were grown by molecular beam epitaxy. The core GaAs nanowires were synthesized under typical nanowire growth conditions using gold as catalyst. For the GaMnAs shell the temperature was drastically reduced to achieve low-temperature growth conditions known to be crucial for high-quality GaMnAs. The GaMnAs shell grows epitaxially on the side facets of the core GaAs nanowires. A ferromagnetic transition temperature of 20 K is obtained. Magnetic anisotropy studies indicate a magnetic easy axis parallel to the nanowire axis.

Combining the growth of ferromagnetic materials with nanowire (NW) growth enables the integration of two important research domains: spintronics and self-assembled nanostructures. With this approach one-dimensional spintronic devices could be realized which will benefit from the specific advantages of the NW growth, such as the large material freedom and the possibility to generate complex axial, radial, or even branched NW heterostructures.[1−4]

Diluted magnetic semiconductors (DMS), with GaMnAs as one of the most extensively studied DMS materials, have attracted great interest because of their promising applications in various spintronic devices.[5−8] In GaMnAs alloys, Mn atoms occupying Ga lattice sites act as acceptors. The Mn atoms thus provide not only the localized magnetic moments but also the holes mediating the ferromagnetic coupling. For the magnetic properties the hole concentration plays a crucial role; e.g., the Curie temperature T_C depends on the hole density as well as on the effective Mn concentration.[9] Since the equilibrium solubility of Mn in GaAs is below 0.1 atom %−a Mn content too low to form ferromagnetism−highly nonequilibrium growth techniques, such as low temperature molecular beam epitaxy (LT-MBE), have been applied.[10] The growth parameters, in particular the substrate temperature, have a strong effect on the crystal quality of GaMnAs. Where growth temperatures are too high, Mn segregation and the formation of MnAs clusters occur.[11] However, at too low substrate temperatures defects such as As antisites or Mn interstitials are formed more frequently, both of which are double donors decreasing the hole concentration of the GaMnAs film and thus reducing T_C. The best growth conditions occur at a substrate temperature slightly below the MnAs segregation threshold in the range of 200−300 °C and by a relatively low As/Ga flux ratio yielding a stoichiometric supply of the two elements.[12−14]

Semiconductor nanowires have been intensively studied due to their great potential for nanoscale electronics and photonics.[4,15] The growth of III−V nanowires using a metal (usually gold) as a catalyst is commonly explained within the vapor−liquid−solid (VLS) mechanism.[16] For a long time chemical vapor deposition (CVD) or chemical beam epitaxy (CBE) were the common techniques used. Molecular beam epitaxy (MBE) has only recently been applied for NW growth.[17−20] NWs can be grown only within a restricted domain of deposition conditions. In the case of Au-assisted MBE growth of GaAs nanowires, the temperature window ranges from 420 to 620 °C.[17]

Since for high-quality GaMnAs the direct approach of growing mixed crystal DMS nanowires via the VLS mechanism[21,22] cannot be applied, we propose to use the core−shell NW concept. This concept is known in particular in the context of surface passivation to improve the optical and

* Corresponding author, elisabeth.reiger@physik.uni-regensburg.de.
[†] University of Regensburg.
[‡] Institute of Physics, Warsaw.
[§] ETH Zurich.

10.1021/nl9020717 CCC: $40.75
Published on Web 09/04/2009

electrical properties in various NW based devices such as NW lasers and NW field effect transistors.[1,23−26] In a first growth step we generate GaAs NWs as nonmagnetic templates, followed by LT-MBE growth of a GaMnAs shell on the NW sidewalls. Our approach can be of course expanded to the growth of other III−Mn−V nanowire structures (e.g., InMnSb nanotubes on InSb or CdTe NWs templates) but also to semiconductor/metallic NW heterostructures such as Fe nanotubes grown on lattice matched GaAs NWs or magnetite core−shell NWs as shown by Zhang et al.[27]

Here we report for the first time the successful integration of a GaMnAs shell in a radial NW heterostructure. We note that in previous studies the growth of GaMnAs nanowires under typical NW, i.e., high temperature conditions, has been reported.[28−30] Sadowski et al.[29] showed that the growth of GaMnAs at MnAs segregation conditions led to the formation of MnAs nanocluster acting as catalyst for the NW growth. The obtained NWs were strongly tapered with side branches. Martelli et al.[30] reported on Mn-assisted GaAs NW growth. Transport measurements indicated that the wires are p-type due to catalyst diffusion into the nanowire. The study did not cover whether the Mn content was sufficiently large to induce a ferromagnetic phase. Recently Kim et al.[28] synthesized GaMnAs nanowires using the vapor transport method with gold as catalyst which exhibited room-temperature ferromagnetism. The highest magnetic moment was reported for a Mn content of 3%. To our knowledge there is no mechanism which could explain above room temperature T_C values for 3% Mn concentration[9]—except for the magnetic proximity effect observed in hybrid Fe/(Ga,Mn)As systems.[31] Furthermore Jeon et al.[32] published data indicating room-temperature ferromagnetism of GaMnAs nanowires with a Mn concentration as high as 20%. The proposed NW growth mechanism based on the formation of (Ga,Mn)As islands seems, however, to be questionable.[29] Care has to be taken that, e.g., the formation of MnAs nanoclusters can be excluded as a possible source for the observed ferromagnetism.[33]

The nanowires in our study were grown by molecular beam epitaxy (MBE) using a modified Veeco Gen II system. The system is equipped with a conventional RHEED-system operating at 15 keV and two infrared pyrometers, one specified for high temperatures (500−1000 °C) and the other for low temperatures (100−700 °C). The given absolute temperature values have an estimated uncertainty of ±10 °C. Prior to the NW growth a thin gold film (typical thickness between 10 and 14 Å) was deposited on the native oxide of a GaAs(111)B substrate in a separate MBE chamber.[34] In order to form the Au catalyst droplets as well as to remove the native oxide, the substrate was heated to 610 °C for approximatively 1 h under As_4 flux. The successful oxide desorption was monitored by RHEED. For the NW growth the temperature was reduced to 540 °C. The Ga rate was set to 0.4 Å/s at an As_4 flux of 1.2×10^{-6} Torr, giving an As_4/Ga flux ratio of 6.[35] The rather high flux ratio leads to a low Ga supersaturation of the catalyst droplets, which favors zinc blende as the crystal structure of the NWs.[36] It also ensures a high density and uniform distribution of the NWs.[37] After 4 h the growth of GaAs NW templates was stopped.

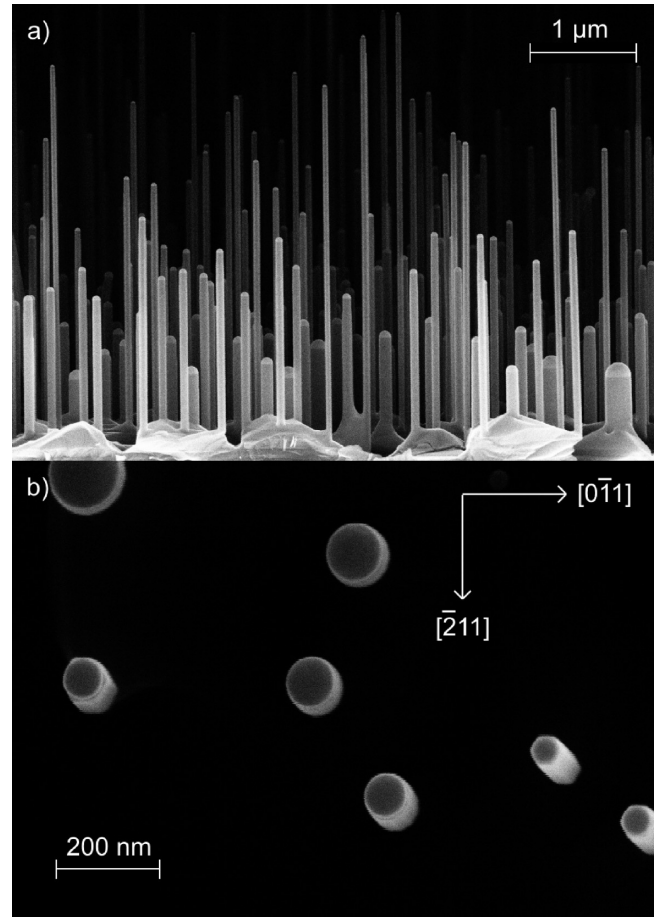

Figure 1. GaAs core NWs: (a) SEM side view. All NWs grow in the [111] direction, perpendicular to the (111)B GaAs substrate plane. (b) SEM top view. In particular NWs with smaller diameters possess a hexagonal cross section with {211}-oriented facets.

The morphology and crystal structure of the NWs were characterized by scanning electron microscopy (SEM) and transmission electron microscopy (TEM). All NWs show a preferential [111] growth direction, perpendicular to the GaAs(111)B substrate plane (cf. Figure 1a). The NWs have a uniform diameter along the whole length. The diameter of the individual NWs varies from 40 to 180 nm.[38] The length of the NWs is between 500 nm and 4.3 μm and shows an inverse quadratic dependence on the diameter, which is a signature of growth by diffusion of adatoms.[18,39] The typical NW density is between 7 and 11 NW/μm^2. The shape of the NWs can be studied by SEM top view images (cf. Figure 1b).

In particular NWs with small diameter (<70 nm) show a hexagonal cross section. The six facets of the NWs are equivalent crystal planes of the {211} orientation.[40] NWs with larger diameter have a cylindrical shape. In previous studies it was shown that the formation of the facets depends on the growth direction, the V/III flux ratio, and the NW diameter, and both the formation of {211} facets and {110} facets have been observed.[41,42] To further investigate the shape of the NWs, TEM cross section samples were prepared.

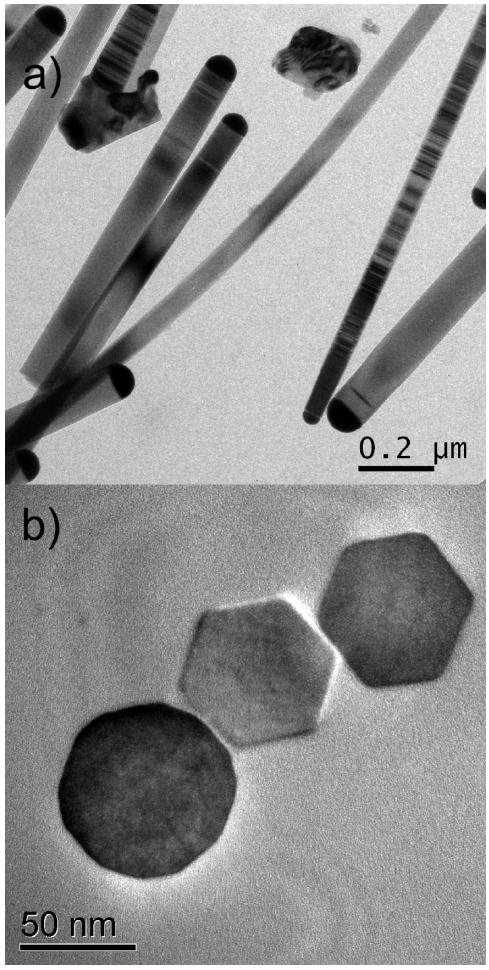

Figure 2. GaAs core NWs: (a) TEM overview image. NWs with a high density of stacking faults as well as almost stacking-fault free NWs are observed. (b) TEM cross section. The NWs have either a hexagonal or a polygonal cross section. From HRTEM images and diffractogram analysis the facets of the hexagonal form are identified to be {211} crystal planes.

The NWs were transferred to a Si substrate and embedded in a SiO layer prior to the standard TEM cross section preparation. In Figure 2b small NWs (diameter 60 and 65 nm) have a hexagonal cross section. From HRTEM images and diffractogram analysis the facets could be identified to be {211}, which is consistent with our SEM analysis. The larger NWs (75 nm diameter) possess a polygonal cross section with 12 facets of the type {211} and {110}.

For III−V NW growth, it is often observed that the NWs crystallize in the wurtzite crystal structure and not in the zinc blende, the bulk crystal structure of GaAs.[41] Typically the NWs contain stacking faults (SF) and/or sections with either the zinc blende or the wurtzite crystal structure. It was shown both theoretically and experimentally that the crystal structure of the NW depends on the group III supersaturation of the catalyst droplet as well as on a critical diameter of the NW.[36,39] Below a certain critical value the formation of wurtzite NWs is with regard to the total energy preferred. Low supersaturation favors the zinc blende structure.

TEM bright field (BF) images of an ensemble of NWs transferred onto a copper grid were used to study the morphology of the NWs. In Figure 2a one can see that the density of SFs is not homogeneously distributed. We observed almost SF-free NWs as well as NWs with a high density of SFs. NWs with a larger diameter generally exhibit a lower density of SFs with zinc blende being the dominant crystal structure as determined by electron diffraction (cf. Figure 4). For thin NWs both zinc blende and wurtzite sections are identified.

For the growth of the core−shell NWs GaAs NWs were grown under identical growth conditions as described above. The substrate temperature was then reduced to below 250 °C. The Ga rate was kept constant at 0.4 Å/s whereas the As_4 flux was set to 0.6×10^{-6} Torr giving a As_4/Ga flux ratio of 3. After temperature stabilization, a GaMnAs shell containing approximately 5% Mn was grown around the GaAs wire.[43] During growth the substrate was rotated at a speed of 7 rounds/min. A temperature series of core−shell NWs was grown with identical growth parameters but increasing substrate temperatures.

In Figure 3 SEM side view images of core−shell NWs grown at (a) 224, (b) 234, and (c) 247 °C are shown. For all samples the same amount of material (corresponding to a 300 nm thick 2D GaMnAs layer) was deposited. Samples a and b depicted in Figure 3 grown at 224 and 234 °C show a GaMnAs shell of high quality with rare cluster formation at the sidewalls. For 247 °C (cf. Figure 3c) branched NW growth is observed. This is most likely caused by the formation of MnAs cluster due to enhanced Mn segregation, similar to the NW growth at MnAs segregation conditions as reported by Sadowski et al.[29] We note that the measured temperature of 247 °C is lower than the typical substrate temperature for which the formation of MnAs precipitates takes place for (100)-oriented GaMnAs 2D layer growth of similar Mn concentration. However, the 2D growth conditions might differ considerably from the growth on the 3D surface of a NW sample. In particular, one has to keep in mind that the temperature at which MnAs precipitates are formed can be substantially lower for the growth on substrate orientation different than (100). Additionally, at the sharp corners being the joints of the NWs facets, as those visible in Figure 2b, MnAs cluster formation could occur preferentially. The formation of MnAs precipitates could also be enhanced at the side facets of NWs by stacking faults and defects in the NWs (cf. Figure 2a). Increasing the substrate temperature further (252 °C) leads also to the formation of thin NW-like structures on the substrate (not shown).

All obtained core−shell NWs have the same shape. At the tip of the NW we still observe GaMnAs axial growth despite the low substrate temperatures where the AuGa catalyst droplet is solid. However this effect is accompanied by strong cluster formation. The thickness of the GaMnAs shell decreases toward the substrate. This is caused by partial blocking of the atomic beam by neighboring NWs. Since the diffusion of the Ga and Mn adatoms is strongly reduced at low temperatures and because of the geometry of the MBE system where the cells are oriented under an angle of $\approx 30°$ with respect to the normal of the sample, this shadowing effect appears for samples with a high density of NWs. We

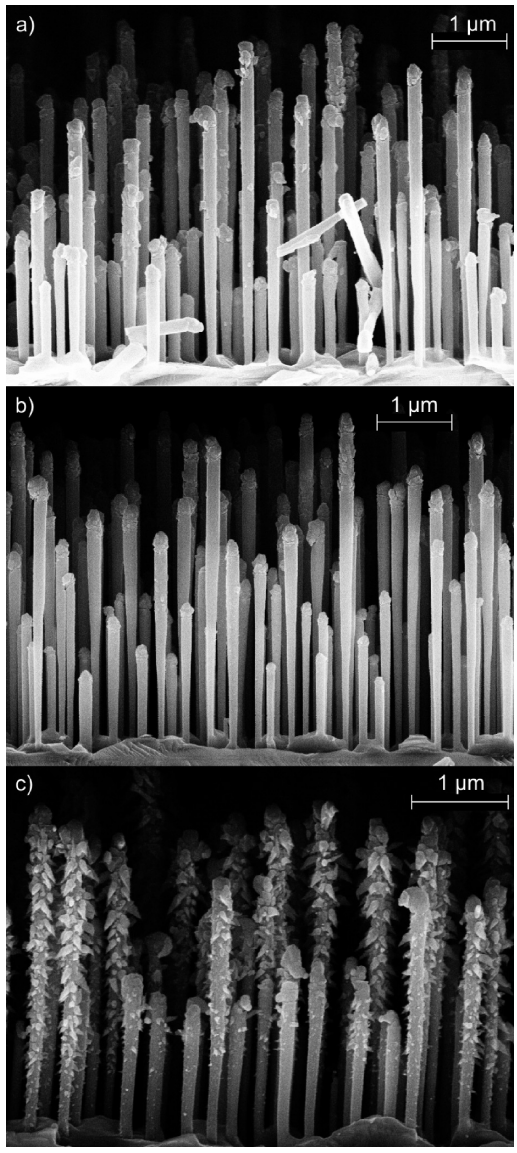

Figure 3. SEM pictures of GaMnAs/GaAs core−shell NWs: The GaMnAs shell was grown with identical growth parameters, but at different substrate temperatures of (a) 224, (b) 234, and (c) 247 °C. A nominal 2D thickness of 300 nm GaMnAs was deposited. Optimal growth takes place at a narrow temperature window around 235 °C. For higher temperatures (247 °C) branched NW growth is observed most probably caused by the formation of MnAs clusters due to Mn segregation.

want to exploit this effect to circumvent or strongly reduce the planar growth of GaMnAs on the substrate in between the NWs. This will become important for the interpretation of SQUID measurements of the as-grown NW samples. Therefore the GaAs core NWs were grown with an average length of 3−3.5 μm. This is within the typical diffusion length of Ga adatoms to ensure the growth of NWs with uniform diameters but sufficiently long to maximize the shadowing effect.

Figure 4a shows a BF-TEM picture of a typical core−shell NW where the GaMnAs shell was deposited at a substrate temperature of 234 °C with a nominal 2D thickness of 300 nm. This NW has a base diameter of 80 nm, a head diameter of 200 nm, and a length of 3.9 μm; i.e., the shell thickness

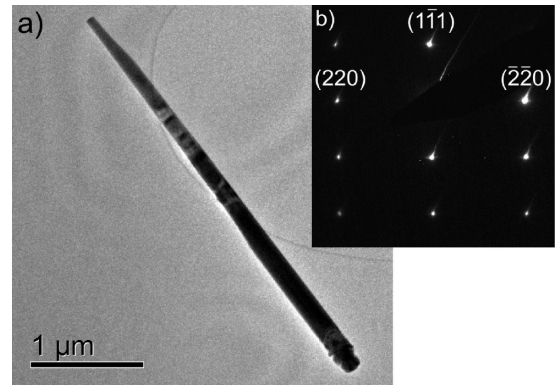

Figure 4. GaAs/GaMnAs core−shell NW with GaMnAs shell grown at 234 °C. (a) TEM picture of a single NW with a base diameter of 80 nm a head diameter of 200 nm and a length of 3.9 μm. (b) Electron diffraction pattern taken at the base of the NW, showing the typical pattern of zinc blende crystal structure with the electron beam aligned along the [11$\bar{2}$] direction.

decreases by 60 nm over the whole length of the NW. Taking 40 nm as the typical diameter of NWs of this length (derived by SEM analysis of GaAs core NWs) the shell thickness at the base (tip) of the NW is approximately 20 nm (80 nm). Electron diffraction pattern taken at the base (cf. Figure 4b) and below the head of the NW confirmed that the core−shell NW crystallized in zinc blende.

Further TEM investigations (cf. Figure S1 in Supporting Information) confirm that the GaMnAs shell grows epitaxially on the sidewalls of the core GaAs NW, adapting to the crystal structure of the core NW. This applies even to SFs of the core GaAs NW which extend into the GaMnAs shell. Most of the parts of the GaMnAs shell are of high quality but also crystal defects within the GaMnAs shell as well as cluster formation at the sidewalls (consistent with SEM characterization) are observed. At the head of the NW, at the AuGa catalyst particle, polycrystalline GaMnAs growth takes place. This polycrystalline region has a typical lateral dimension of 200−300 nm.

The magnetic characterization was carried out by a superconducting quantum interference device (SQUID). All NW samples were characterized as-grown. As the NWs grow preferentially along the [111] direction (cf. Figure 3) the magnetic field can thus be oriented with respect to the NW axis. Due to the high density of NWs and an average length of 3.5 μm, the planar growth of GaMnAs on the substrate is almost completely suppressed. For an idealized NW sample with a uniform NW diameter of 70 nm, a NW length of 3.5 μm, and a NW density of 10 NW/μm^2, the total surface area of the NWs would be factor 7.7 larger than the bare substrate surface. Assuming that the GaMnAs would be equally distributed over the total area, this would result in a shell thickness of 34 and 23 nm for a nominal 2D thickness of 300 or 200 nm, respectively. In reality due to the reduced diffusion of adatoms the percentage of GaMnAs material deposited at the tip of the NWs will be even higher and, as a consequence, the planar growth even more inhibited. This is consistent with SEM characterizations of core−shell NWs where the obtained base shell thickness of <20 nm was

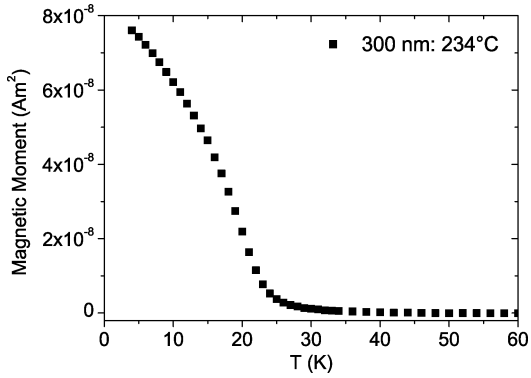

Figure 5. Temperature dependence of magnetization of a core−shell NW sample grown at 234 °C with a nominal GaMnAs 2D thickness of 300 nm giving a Curie temperature T_C of 20 K. For the measurement an external field of 250 Oe parallel to the NW axis along the [111]direction was applied.

considerably thinner than the calculated value of 34 nm. Therefore the magnetization values obtained by SQUID measurements can be attributed mainly to the magnetic shell of the NWs with the contribution of the planar grown GaMnAs in between the NWs being at most 10% of the signal.

The Curie temperature T_C was determined by measuring the temperature dependence of the magnetization with a magnetic field of 250 Oe applied parallel to the NW axis along the [111] direction. NW samples with a nominal GaMnAs 2D thickness of 200 or 300 nm grown at substrate temperatures between 224 and 247 °C were analyzed. All NW samples show T_C values in the range of 12 and 20 K. The highest T_C of 20 K is achieved for growth temperatures of 231 and 234 °C for a nominal 2D GaMnAs thickness of 200 or 300 nm, respectively (cf. Figure 5). The thickness of the GaMnAs shell does not have a measurable effect on T_C. Increasing the growth temperature (241 °C) as well as decreasing the growth temperature (224 °C) leads to lower T_C values of 17 or 16 K. At 247 °C substrate temperature where branched NW growth starts to take place, T_C is reduced to 12 K, indicating a reduced quality and a possible lower Mn content of the GaMnAs shell.

It is known that T_C of GaMnAs films depends strongly on the crystal orientation of the substrate. The current record of T_C close to 180 K has been reported for a GaMnAs film with 11% Mn concentration grown on a (001) GaAs substrate with an improved postgrowth annealing technique.[44,45] Note that T_C of the as-grown sample was 85 K in this case. For the crystal orientations (311)A, (110), (201), (110), and (411)A the achieved T_C of the as-grown as well as annealed samples were considerably lower, with the (110) orientation exhibiting the lowest T_C values.[4613,14,47−49] To date no reference data for GaMnAs films grown on (211) substrates are available.

As the GaMnAs shell is grown on the side facets of the core NWs which consist of either {211} planes (for the hexagonal cross section) or of {211} and {110} planes (for the polygonal shaped NWs), the low T_C value is probably caused by the specific crystal orientation. The nonuniform

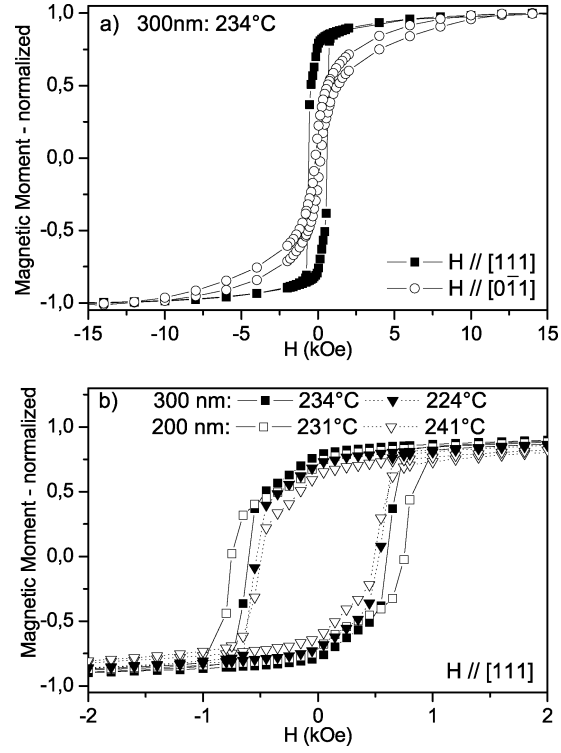

Figure 6. (a) Magnetization hysteresis loops at 6 K of a NW sample with a GaMnAs shell of a nominal 2D thickness of 300 nm, grown at 234 °C. The magnetic field is applied parallel to the NW axis in [111] direction or perpendicular to the NW axis in [1$\bar{1}$0] direction. (b) Magnetization hysteresis loops at 6 K with magnetic field applied along the NW axis ([111] direction) for different NW samples grown at 224−241 °C with a nominal GaMnAs 2D thickness of 200 or 300 nm. All NW samples show the same characteristic behavior.

shell thickness could have an additional effect. In particular at the tip of the NW with the thickest shell, enhanced Mn segregation and cluster formation (as seen by SEM characterization) could lead to a reduction of T_C.[50] For a uniform core NW sample, generated, e.g., by position and size controlled NW growth[51] with well-defined side facets, it should be feasible to further optimize the GaMnAs growth parameters yielding higher T_C values.

In Figure 6a, magnetization hysteresis loops of a NW sample with a GaMnAs shell of a nominal 2D thickness of 300 nm grown at 234 °C are shown. The magnetic field was applied either parallel to the NW axis along the [111] direction or perpendicular to the NW axis in the [0$\bar{1}$1] direction. There is a clear difference between the two field orientations. In the perpendicular case the NWs show a magnetic hard axis behavior with 20% remanence at zero field and almost no hysteresis. In the parallel field orientation the remanence is 80% and a coercive field of 550 Oe is observed. For the parallel field orientation various NW samples with two different GaMnAs nominal 2D thicknesses grown at different substrate temperatures are compared (cf. Figure 6b). All NW samples exhibit the same characteristics. The remanence at zero magnetic field is between 80% and 65%. The coercive fields range from 500 to 750 Oe with the NW samples with higher Curie temperatures having a larger coercive field. The magnetization hysteresis loops

show that the [111] direction parallel to the NW axis is a magnetic easy axis. For the branched NW sample we observe, as expected, a less pronounced magnetic anisotropy (cf. Figure S2 in Supporting Information). For a full understanding of the hysteresis loops, one also has to take into account that the magnetic signal arising from the (not totally suppressed) planar growth in between the NWs and from the polycrystalline GaMnAs growth at the tip of the NWs contribute to the signal. Furthermore, there are a finite number of kinked NWs. (The reason is that the sample cannot be mounted in the SQUID without NWs at the edge of the sample breaking off.) Third, due to the nonuniform shell thickness the anisotropy constants are likely to vary along the NW axis. All three points explain to some extent the observed deviation of Figure 6b from the squared loop characteristics of an ideal magnetic easy axis.

The magnetic anisotropy of GaMnAs films is complex. Usually it consists of a cubic anisotropy term of the GaMnAs zinc blende structure superimposed with additional uniaxial anisotropy terms.[52] Anisotropy studies are mainly performed on (001) oriented GaMnAs films, but also (311) GaMnAs and (110) GaMnAs films have been studied.[14,53] However, no data are available for the (211) orientation. It has been shown that the magnetic anisotropy of (001) GaMnAs films is largely controlled by epitaxial strain, which can also be used to engineer the anisotropy by, e.g., lithographical strain relaxation.[54,55]

The core−shell NW approach produces GaMnAs nanotubes with nonmagnetic GaAs cores, which would ideally consist of six equivalent {211} planes. As shown for lithographically generated GaMnAs stripes of similar width, shape anisotropy terms do not play a significant role as the saturation magnetization is small.[54,56] Two basic scenarios are thought to be possible. Either a uniform magnetization forms with a well-defined magnetic anisotropy or the different side facets develop separate magnetic domains which add up to a net magnetization. In the second scenario one would expect a net magnetization pointing along the NW axis as radial components of opposite side facets cancel each other out. This is valid, when the magnetic easy axis of the side facets does not point perpendicularly to the NW axis, which can be excluded from our measurements. For the uniform magnetization, although no simulation of strain induced anisotropy of (211) GaMnAs stripes exist, we expect the reason for the observed easy axis along the NW axis to be the same as in the case of lithographically defined stripes, namely, anisotropic strain relaxation.[54,55] Further studies are required to fully understand the magnetic anisotropy of the GaMnAs nanotubes.

In conclusion, we have successfully combined the growth of ferromagnetic GaMnAs with GaAs NWs. Using the core−shell NW approach the GaMnAs shell was deposited on the side facets of GaAs NWs under low temperature conditions. The GaMnAs grows epitaxially on the GaAs NWs with good crystal quality. The maximum achieved Curie temperature is 20 K. However, using more uniform GaAs NW templates, realized by position and diameter controlled NW growth and including templates from GaAs NWs having growth axis different from [111], the growth conditions of the GaMnAs shell can be further optimized and higher Curie temperatures should be possible to obtain. The NWs show a strong magnetic anisotropy. Our results constitute an important step toward the realization of spintronic semiconductor nanodevices utilizing the bottom-up approach.

Acknowledgment. The authors thank G. Bayreuther, M. Sawicki, K. Lebecki, and A. Fontcuberta i Morral for discussions. We acknowledge financial support from the Deutsche Forschungsgemeinschaft via SFB 689. The research in Poland was partially supported by the European Union within European Regional Development Fund, through grant Innovative Economy (POIG.01.01.02-00-008/08), and by the Foundation for Polish Science through subsidy 12/2007.

Supporting Information Available: Further TEM analysis of GaMnAs/GaAs core−shell NWs is provided, and magnetization hysteresis loops of the branched GaMnAs core−shell NW sample, with the GaMnAs shell grown at 247 °C, and the NW sample showing the highest T_C, with the GaMnAs shell deposited at 234 °C, are compared. This material is available free of charge via the Internet at http://pubs.acs.org.

References

(1) Lauhon, L. J.; Gudiksen, M. S.; Wang, D.; Lieber, C. M. *Nature* **2002**, *420*, 57.
(2) Lu, W.; Lieber, C. M. *Nat. Mater.* **2007**, *6*, 841–850.
(3) Wang, D.; Quian, F.; Yang, C.; Zhong, Z.; Lieber, C. M. *Nano Lett.* **2004**, *4*, 871–874.
(4) Thelander, C.; Agarwal, P.; Brongersma, S.; Eymery, J.; Feiner, L. F.; Forchel, A.; Scheffler, M.; Riess, W.; Ohlsson, B. J.; Gösele, U.; Samuelson, L. *Mater. Today* **2006**, *9*, 28–35.
(5) Furdyna, J. K. *J. Appl. Phys.* **1988**, *64*, R29.
(6) Ohno, H.; Munekata, H.; Penny, T.; Molnar, S. V.; Chang, L. L. *Phys. Rev. Lett.* **1992**, *68*, 2664.
(7) Ohno, H. *Science* **1998**, *281*, 951.
(8) *Semiconductors and Semimetals: Spintronics*; Dietl, T., Awschalom, D. D., Kaminska, M., Ohno, H., Eds.; Elsevier: Oxford, 2008; Vol. 82.
(9) Dietl, T.; Ohno, H.; Matsukura, F. *Phys. Rev. B* **2001**, *63*, 195205.
(10) Ohno, H.; Shen, A.; Matsukura, F.; Oiwa, A.; Endo, A.; Katsumoto, S.; Iye, Y. *Appl. Phys. Lett.* **1996**, *69*, 363.
(11) Hayashi, T.; Tanaka, M.; Nishinaga, T.; Shimada, H.; Tsuchiya, H.; Otuka, Y. *J. Cryst. Growth* **1997**, *175−176*, 1063.
(12) Campion, R. P.; Edmonds, K. W.; Zhao, L. X.; Wang, K. Y.; Foxon, C. T.; Gallagher, B. L.; Staddon, C. R. *J. Cryst. Growth* **2003**, *247*, 42.
(13) Wurstbauer, U.; Sperl, M.; Schuh, D.; Bayreuther, G.; Sadowski, J; Wegscheider, W. *J. Cryst. Growth* **2007**, *301−302*, 260–263.
(14) Wurstbauer, U.; Sperl, M.; Soda, M.; Neumaier, D.; Schuh, D.; Bayreuther, G.; Zweck, J.; Wegscheider, W. *Appl. Phys. Lett.* **2008**, *92*, 102506.
(15) Minot, E. D.; Kelkensberg, F.; van Kouwen, M.; van Dam, J. A.; Kouwenhoven, L. P.; Zwiller, V.; Borgström, M. T.; Wunnicke, O.; Verheijen, M. A.; Bakkers, E. P. A. M. *Nano Lett.* **2007**, *7*, 367–371.
(16) Wagner, R. S.; Ellis, W. C. *Appl. Phys. Lett.* **1964**, *4*, 89.
(17) Harmand, J.; Tchernycheva, M.; Patriarche, G.; Travers, L.; Glas, F.; Cirlin, G. *J. Cryst. Growth* **2007**, *301−302*, 853–856.
(18) Dubrovskii, V.; Sibirev, N. V. *J. Cryst. Growth* **2007**, 504–513.
(19) Tchernycheva, M.; Travers, L.; Patriarche, G.; Harmand, J. C.; Cirlin, G. E.; Dubrovskii, V. G. *J. Appl. Phys.* **2007**, *102*, 094313.
(20) Fontcuberta i Morral, A.; Colombo, C.; Abstreiter, G.; Arbiol, J.; Morante, J. R. *Appl. Phys. Lett.* **2008**, *92*, 063112.
(21) Radovanovic, P. V.; Barrelet, C. J.; Gradečak, S.; Qian, F.; Lieber, C. M. *Nano Lett.* **2005**, *5*, 1407–1411.
(22) Zaleszczyk, W.; Janik, E.; Presz, A.; Dłużewski, P.; Kret, S.; Szuszkiewicz, W.; Morhange, J.-F.; Dynowska, E.; Kirmse, H.;

Neumann, W.; Petroutchik, A.; Baczewski, L. T.; Karczewski, G.; Wojtowicz, T. *Nano Lett.* **2008**, *8*, 4061–4065.
(23) Hua, B.; Motohisa, J.; Kobayashi, Y.; Hara, S.; Fukui, T. *Nano Lett.* **2009**, *9*, 112–116.
(24) Xiang, J.; Lu, W.; Lu, Y.; Wu, Y.; Yan, H.; Lieber, C. M. *Nature* **2006**, *441*, 489.
(25) Jiang, X.; Xiong, Q.; Nam, S.; Quian, F.; Li, Y.; Lieber, C. M. *Nano Lett.* **2007**, *7*, 3214–3218.
(26) Bryllert, T.; Wernersson, L. E.; Froberg, L. E.; Samuelson, L. *IEEE Electron Device Lett.* **2006**, *27*, 323.
(27) Zhang, D.; Liu, Z.; Han, S.; Li, C.; Lei, B.; Stewart, M. P.; Tour, J. M.; Zhou, C. *Nano Lett.* **2004**, *4*, 2151–2155.
(28) Kim, H. S.; Cho, Y. J.; Kong, K. J.; Kim, C. H.; Chung, G. B.; Park, J. *Chem. Mater.* **2009**, *21*, 1137–1143.
(29) Sadowski, J.; Dłużewski, P.; Kret, S.; Janik, E.; ŁLusakowska, E.; Kanski, J.; Presz, A.; Terki, F.; Charar, S.; Tang, D. *Nano Lett.* **2007**, *7*, 2724–2728.
(30) Martelli, F.; Rubini, S.; Piccin, M.; Bais, G.; Jabeen, F.; Franceschi, S. D.; Grillo, V.; Carlino, E.; D'Acapito, F.; Boscherini, F.; Cabrini, S.; Lazzarino, M.; Businaro, L.; Romanato, F.; Franciosi, A. *Nano Lett.* **2006**, *6*, 2130–2134.
(31) Maccherozzi, F.; Sperl, M.; Panaccione, G.; Minar, J.; Polesya, S.; Ebert, H.; Wurstbauer, U.; Hochstrasser, M.; Rossi, G.; Woltersdorf, G.; Wegscheider, W.; Back, C. H. *Phys. Rev. Lett.* **2008**, *101*, 267201.
(32) Jeon, H. C.; Kang, T. W.; Kim, T. W.; Yu, Y.-J.; Jhe, W.; Song, S. A. *J. Appl. Phys.* **2007**, *101*, 023508.
(33) Moreno, M.; Trampert, A.; Däweritz, L.; Ploog, K. H. *Appl. Surf. Sci.* **2004**, *234*, 16–21.
(34) The deposition of thin Au film by metal MBE was done in the Institute of Physics, Warsaw, by A. Petroutchik and L. T. Baczewski.
(35) The As_4/Ga flux ratio can be calculated from the beam equivalent pressure of both beams taking into account the absolute temperatures, molecular weight, and the ionization efficiency relative to nitrogen of the two specimens .
(36) Glas, G. P.; Harmand, J. *Phys. Rev. Lett.* **2007**, *99*, 146101.
(37) Plante, M. C.; LaPierre, R. R. *Nanotechnology* **2008**, *19*, 495603.
(38) This large variation in the diameter is typical for the thin film Au technique, where the diameter of the catalyst particles determining the size of the NWs shows a large statistical spreading. The variance in diameter, however, depends on the oxide desorption parameters as well as on the thickness of the Au film and can be tuned by adjusting these parameters.
(39) Dubrovskii, V. G.; Sibirev, N. V.; Harmand, J. C.; Glas, F. *Phys. Rev. B* **2008**, *78*, 235301.
(40) The six side facets of the NWs are a subset of the crystal plane class {211}, with the [111] direction being parallel to the planes, namely, $(\bar{2}11)$, $(\bar{1}\bar{1}2)$, $(1\bar{2}1)$, $(2\bar{1}\bar{1})$, $(11\bar{2})$, and $(\bar{1}2\bar{1})$.
(41) Mariager, S. O.; Sorensen, C. B.; Aagesen, M.; Nygard, J.; Feidenhans, R. *Appl. Phys. Lett.* **2007**, *91*, 083106.
(42) Plante, M.; LaPierre, R. *J. Cryst. Growth* **2006**, *286*, 394–399.
(43) The Mn flux was determined by RHEED oscillations of 2D growth of MnAs films on (001) GaAs for various temperatures of the Mn cell. With the obained correlation, the Mn flux and hence the Mn concentration for the specific Mn cell temperature used during NW growth could be estimated.
(44) Olejnik, K.; Owen, M. H. S.; Novak, V.; Masek, J.; Irvine, A. C.; Wunderlich, J.; Jungwirth, T. *Phys. Rev. B* **2008**, *78*, 054403.
(45) Edmonds, K. W.; Boguslawski, P.; Wang, K. Y.; Campion, R. P.; Novikov, S. N.; Farley, N. R. S.; Gallagher, B. L.; Foxon, C. T.; Sawicki, M.; Dietl, T.; Nardelli, M. B.; Bernholc, J. *Phys. Rev. Lett.* **2004**, *92*, 037201.
(46) An orientation-dependent efficiency of Mn incorporation and/or an orientation-dependent As antisite defect density are discussed as possible reasons for the reduced T_C values. For the (110) orientation a maximum T_C of 65 K for 6% Mn concentration could be achieved (cf. ref 14).
(47) Wilson, M. J.; Xiang, G.; Sheu, B. L.; Schiffer, P.; Sarmarth, N.; May, S. J.; Bhattacharya, A. *Appl. Phys. Lett.* **2008**, *93*, 262502.
(48) Omiya, T.; Matsukura, F.; Shen, A.; Ohno, Y.; Ohno, H. *Physica E* **2001**, *10*, 206–209.
(49) Wang, K. A.; Edmonds, K. W.; Zhao, L. X.; Sawicki, M.; Campion, R. P.; Gallagher, B. L.; Foxon, C. T. *Phys. Rev. B* **2005**, *72*, 115207.
(50) Singh, A. *Phys. Rev. B* **2007**, *75*, 035206.
(51) Fan, H. J.; Werner, P.; Zacharias, M. *Small* **2006**, *2*, 700–717.
(52) Gould, C.; et al. *New J. Phys.* **2008**, *10*, 055007.
(53) Bihler, C.; Huebl, H.; Brandt, M. S.; Goennenwein, S. T. B.; Reinwald, M.; Wurstbauer, U.; Döppe, M.; Weiss, D.; Wegscheider, W. *Appl. Phys. Lett.* **2006**, *89*, 012507.
(54) Hümpfner, S.; Pappert, K.; Wenisch, J.; Brunner, K.; Gould, C.; Schmidt, G.; Molenkamp, L. W.; Sawicki, M.; Dietl, T. *Appl. Phys. Lett.* **2007**, *90*, 102102.
(55) Wenisch, J.; Gould, C.; Ebel, L.; Storz, J.; Pappert, K.; Schmidt, M. J.; Kumpf, C.; Schmidt, G.; Brunner, K.; Molenkamp, L. *Phys. Rev. Lett.* **2007**, *99*, 077201.
(56) Bihler, C.; Althammer, M.; Brandlmaier, A.; Geprägs, S.; Weiler, M.; Opel, M.; Schoch, W.; Limmer, W.; Gross, R.; Brandt, M. S.; Goennenwein, S. T. B. *Phys. Rev. B* **2008**, *78*, 045203.

NL9020717